Inorganic Chemistry

Article

pubs.acs.org/IC

Theoretical Study of Bond Distances and Dissociation Energies of Actinide Oxides AnO and AnO_2

Attila Kovács,*[,†,‡] Peter Pogány,[†] and Rudy J. M. Konings[†]

[†]European Commission, Joint Research Centre, Institute for Transuranium Elements, P.O. Box 2340, 76125 Karlsruhe, Germany

[‡]Department of Inorganic and Analytical Chemistry, Budapest University of Technology and Economics, H-1111 Budapest, Szt. Gellért tér 4, Hungary

Supporting Information

ABSTRACT: In the present study we evaluated trends in the bond distances and dissociation enthalpies of actinide oxides AnO and AnO_2 (An = Th−Lr) on the basis of consistent computed data obtained by using density functional theory in conjunction with relativistic small-core pseudopotentials. Computations were carried out on AnO (An = Th−Lr) and AnO_2 (An = Np, Pu, Bk−Lr) species, while for the remaining AnO_2 species recent literature data (*Theor. Chem. Acc.* **2011**, *129*, 657) were utilized. The most important computed properties include the geometries, vibrational frequencies, dissociation enthalpies, and several excited electronic states. These molecular properties of the late actinide oxides (An = Bk−No) are reported here for the first time. We present detailed analyses of the bond distances, covalent bonding properties, and dissociation enthalpies.

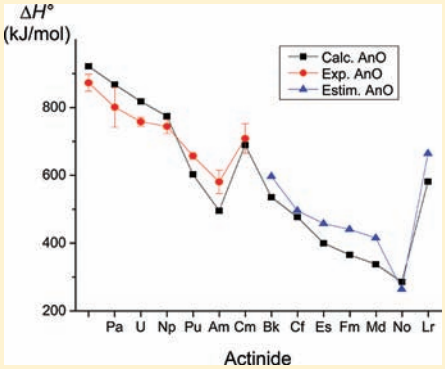

1. INTRODUCTION

The oxides are fundamental compounds of actinides: their long-lived isotopes can generally be found as oxides in nature, their production ends, and their utilization starts mostly from oxides. Not surprisingly, the most studied actinide compounds are the solid oxides AnO, AnO_2, and An_2O_3.[1,2] The (considerably fewer) experimental results on gaseous actinide oxides are reviewed by Heaven et al.[3,4] The body of experimental and theoretical information on the oxides of the early actinides has facilitated the evaluation of trends in various physicochemical properties.[2,5,6] Because of the lack of data, however, these trends are generally cut around the border of early and late actinides.

Very limited information has been gleaned for the late actinides owing to their very short lifetimes, the same reason these elements are not present in nature. The electronic ground states, a few excited states, and the ionization energies of Bk−No have been determined in spectroscopic studies,[7−9] while a limited number of compounds (oxides, halides, organometallic complexes) of Bk, Cf, and Es have been synthesized and studied.[1,2,10,11] The missing experimental information on the dissociation energies of monoxides and vaporization properties of sesquioxides was substituted by estimates on the basis of analogy with certain lanthanide properties.[12−14]

The enormous experimental difficulties of studying these species and associated uncertainties valorize the role of quantum chemical modeling. However, until now theoretical investigations have been focused on the early actinides, especially Th and U. Numerous studies have been published on their small molecules and organometallic complexes, and the literature is particularly extensive for their oxides.[15]

In contrast, theoretical studies on late actinide compounds are very rare, in spite of the theoretical tools available from the mid 1990s.[16,17] The tools include both all electron basis sets, such as used in the Amsterdam Density Functional package,[18] and relativistic small-core pseudopotentials with appropriate valence basis sets.[19] The pseudopotentials, extended recently with larger valence basis sets,[20,21] have been used to predict the bond lengths, binding energies, and vibrational constants of LrH, LrO, and LrF.[21]

The present study deals with gaseous actinide oxide molecules and is primarily of theoretical interest, as the late actinides do not have many applications. The main goal is the evaluation of the trends in bond distances and dissociation enthalpies of AnO and AnO_2 oxides along the actinide row, contributing in this way to the understanding of the fundamental properties of actinides. For the oxides of early actinides we utilize both previous[22] and presently computed data. For the oxides of late actinides (except LrO) our study provides the first information on their basic physicochemical molecular properties.

For the computational method we chose the B3LYP exchange-correlation functional[23,24] in conjunction with small-core pseudopotentials.[19−21] Our preference for this theoretical level is reasoned by the following good experience: (i) it was one of the best performing methods for the early actinide (Th−Cm) oxides in comparative studies testing various exchange-correlation functionals;[15,22] (ii) the average deviation from experimental data on the ionization energies of AnO and AnO_2

Received: February 6, 2012
Published: April 3, 2012

Table 1. Comparison of Various Theoretical Levels for the First Ionization Energies (eV) of the Late Actinides

An	ground state atom[a]	ground state ion[a]	expt[a]	B3LYP	CASSCF[b]	ACPF + SO[b]	CCSD(T)[c]
Bk	$5f^97s^2$	$5f^97s^1$	6.1979(2)	6.23	4.98	5.93	
Cf	$5f^{10}7s^2$	$5f^{10}7s^1$	6.2817(2)	6.29	5.08	5.99	
Es	$5f^{11}7s^2$	$5f^{11}7s^1$	6.3676(5)	6.39	5.21	6.08	
Fm	$5f^{12}7s^2$	$5f^{12}7s^1$	6.50(7)	6.57	5.34	6.18	
Md	$5f^{13}7s^2$	$5f^{13}7s^1$	6.58(3)	6.72	5.41	6.25	6.38
No	$5f^{14}7s^2$	$5f^{14}7s^1$	6.65(3)	6.68	5.51	6.33	6.45
av error				0.05	1.17	0.30	0.20

[a]The data of Bk, Cf, and Es were taken from ref 9 while the rest came from refs 7 and 8. [b]From ref 21. ACFP means the multireference averaged coupled-pair functional method.[49] [c]From ref 20.

(note that several data had large experimental errors) was relatively small, 0.24 eV;[22] (iii) the average deviation from experimental data on the dissociation enthalpies of AnO_2 (again several with large experimental error) was also relatively small, 30 kJ/mol;[22] (iv) the average deviation of AnO_2 bond distances from those obtained using CASPT2 calculations was 0.016 Å;[15] (v) in the only found theoretical study on a late actinide oxide (LrO) the B3LYP data were in excellent agreement with those obtained at the CCSD(T) level.[21]

Theoretical data on the dioxides of early actinides obtained at our chosen theoretical level have been published recently.[15,22] We took these data for our compilation, except those of NpO_2 and PuO_2. For these two molecules DFT predicted other electronic states lower in energy than the ground states from previous relativistic multiconfigurational computations,[25,26] and in the benchmark analysis in ref 22, the DFT ground states have been considered. In the present study, however, the ground states obtained by sophisticated relativistic CASPT2 calculations are used as the reference; hence, we calculated them here at the DFT level. In addition, molecular properties of the early actinide AnO species have been calculated in the present study on the basis of their previously reported CASPT2 electronic ground states.[25,26]

2. COMPUTATIONAL DETAILS

Our calculations have been performed with the codes Gaussian 03[27] and Gaussian 09[28] for Th−Md and No−Lr oxides, respectively, using the B3LYP exchange-correlation functional.[23,24] For the actinides we used the Cologne−Stuttgart small-core relativistic effective core potentials (ECP60MWB)[19,29] in conjunction with a 14s13p10d8f6g valence basis set contracted to 10s9p5d4f3g (ECP60MWB_SEG basis).[20,21] For oxygen the correlation-consistent aug-cc-pVTZ basis set[30] was applied. Our calculations on the early actinide oxides were performed on the reported electronic ground states of these species.[25] For the oxides of late actinides, however, this information is not available; therefore, we elucidated their electronic ground states in the present study. The obtained electronic states were identified by population analysis followed by swapping occupied and virtual orbitals in order to probe all the possible orbital populations. The minimum character of the optimized geometries was checked by frequency analysis. The natural atomic charges and Wiberg bond indices[31] were determined by Natural Bond Orbital analysis[32] using the NBO 5.G code. The Wiberg bond index is a wave function-based approach using the components of the density matrix for estimation of the bond order (number of covalent bonds formed) in molecules.[33,34] Test calculations performed for basis set superposition error using the counterpoise method[35,36] indicated BSSE for the dissociation energies below 2 kJ/mol.

3. RESULTS AND DISCUSSION

Because no information is available on the performance of our chosen computational level for late actinides, we started with a test of their first atomic ionization energies. Experimental data are available for An = Bk−No, though that of Fm is only a semiempirical estimate.[7−9]

The results of our atomic calculations on the experimentally verified ground states are compiled in Table 1. The overall agreement (average error 0.05 eV) is very good, supporting the reliability of our computational level for late actinides. Our present computed results can be compared to those obtained using the same pseudopotential and valence basis set in state-averaged CASSCF and multireference averaged coupled-pair functional (ACPF) calculations, the latter extended with a treatment of spin−orbit effects.[21] In the literature there are also a few CCSD(T) results available on the basis of symmetry broken HF solutions.[20] As the average errors in Table 1 show, from the four methods the B3LYP exchange-correlation functional provided the best performance for the ionization energies.

The electronic ground states of the light actinide monoxides and dioxides have been discussed in detail recently.[25] In the following we present the electronic characteristics of the most stable states from the relevant spin multiplicities of AnO and AnO_2 (An = Bk−Lr) molecules on the basis of our B3LYP calculations. The data are compiled in Tables 2 and 3, respectively.

Except for LrO, two spin multiplicities are found to have low-lying electronic states for the monoxides (cf. Table 2). In the Bk, Cf, and Es monoxides the electronic ground state obtained at our theoretical level belongs to the larger spin multiplicity (8, 7, and 6, respectively), in which all the 5f orbitals are occupied either by one or two electrons, while the 7s orbital is singly occupied. The higher-energy states with spin multiplicities 6, 5, and 4, respectively, are within 20 kJ/mol of the ground-state, the energy difference decreasing from Bk to Es. In EsO the energy difference between the lowest-energy states of spin multiplicities 6 and 4 is marginal; therefore, the ground-state character of spin multiplicity 6 is tentative. The smaller spin multiplicities provide the ground states in the Fm−Lr monoxides. The energy differences of the first excited states from the ground state increase from Fm to Lr. The other spin-multiplicity states are generally higher by more than 100 kJ/mol.

For the dioxides the variation of the electronic ground states is more regular than for the monoxides. From BkO_2 to NoO_2, the ground states have gradually decreasing spin multiplicity (from 6 to 1). In these states the 7s orbital of An is empty, while the β-population (electrons with the opposite spin) of the 5f orbitals is increasing gradually from BkO_2 to NoO_2 (cf. Table 3). Electronic states from other spin multiplicities lie above the ground state by more than 54 kJ/mol, that is, higher than found for the monoxides.

dx.doi.org/10.1021/ic300275y | Inorg. Chem. 2012, 51, 4841−4849

Table 2. Most Stable States of the Relevant Spin Multiplicities (m) of AnO Molecules

m	ΔE^a	1-electron orbitals[b]
		Bk
8	0.0	5fσ, 2 × 5fπ, 2 × 5fδ, 5fϕ, 7s
6	20.4	5fσ, 2 × 5fπ, 2 × 5fδ, 5fϕ, $7s^{\beta}$
4	225.6	5fπ, 2 × 5fδ, 5fϕ, $7s^{\beta}$
10	256.7	6dδ, 5fσ, 2 × 5fπ, 2 × 5fδ, 2 × 5fϕ, 7s
		Cf
7	0.0	5fσ, 2 × 5fπ, 5fδ, 5fϕ, 7s
5	14.0	5fσ, 2 × 5fπ, 5fδ, 5fϕ, $7s^{\beta}$
3	237.5	2 × 5fπ, 5fϕ, $7s^{\beta}$
9	336.7	6dδ, 5fσ, 2 × 5fπ, 2 × 5fδ, 5fϕ, 7s
		Es
6	0.0	5fσ, 5fδ, 2 × 5fϕ, 7s
4	0.2	5fσ, 2 × 5fπ, 5fδ, $7s^{\beta}$
2	102.0	$5fσ^{\beta}$, 5fπ, 5fδ, 5fϕ, $7s^{\beta}$
8	418.5	6dδ, 5fσ, 5fπ, 5fδ, 5fϕ, 7s, O2p
		Fm
3	0.0	5fσ, 5fδ, 5fϕ, $7s^{\beta}$
5	17.8	5fσ, 5fδ, 5fϕ, 7s
1	182.9	
		Md
2	0.0	5fπ
4	64.2	5fσ, 5fπ, 7s
6	547.4	2 × 5fπ, 7s, 7p, O2p
		No
1	0.0	
3	65.3	7s, O2p
5	594.7	6dσ, 7s, 2 × O2p
		Lr
2	0.0	7s
4	344.0	6dδ, 7s, O2p
6	916.8	2 × 6dδ, 7s, 2 × O2p

[a]Relative energy in kJ/mol. [b]The singly populated O2p orbitals have a lone pair character.

Table 3. The Most Stable States of the Relevant Spin Multiplicities (m) of AnO_2 Molecules

m	ΔE^a	1-electron orbitals[b]
		Bk
6	0.0	2 × 5fπ, 5fδ, 2 × 5fϕ
8	76.9	2 × 5fπ, 2 × 5fδ, 2 × 5fϕ, 7s
4	153.4	$5fπ^{\beta}$, 5fπ, 2 × 5fδ, 5fϕ
		Cf
5	0.0	2 × 5fπ, 5fδ, 5fϕ
7	124.9	2 × 5fπ, 2 × 5fδ, 5fϕ, 7s
3	185.0	5fπ, 5fϕ
9	269.8	5fσ, 2 × 5fπ, 2 × 5fδ, 5fϕ, 6dπ, 7s, $7p^{\beta}$, O2s
		Es
4	0.0	2 × 5fπ, 5fϕ
2	82.9	$5fπ^{\beta}$, 5fπ, 5fϕ
6	97.5	5fπ, 2 × 5fδ, 5fϕ, 6dπ
8	357.1	5fδ, 2 × 5fϕ, 7s, 3 × O2p
		Fm
3	0.0	5fπ, 5fϕ
5	54.7	5fπ, 5fδ, 5fϕ, O2p
1	172.7	
7	369.1	2 × 5fδ, 7s, 3 × O2p
		Md
2	0.0	5fδ
4	58.2	3 × O2p
6	312.1	5fϕ, 7s, 3 × O2p
		No
1	0.0	
3	75.5	5fϕ, $7s^{\beta}$, 2 × O2p
5	305.3	4 × O2p
		Lr
2	0.0	O2p
4	213.0	3 × O2p

[a]Relative energy in kJ/mol. [b]The singly populated O2p orbitals have a lone pair character.

In the following we discuss the molecular properties of the electronic ground states of the mono- and dioxides (An = Th−Lr). These are the molecular geometries and bonding characteristics as well as the dissociation energies.

We start with a general description of the bonding as this is the basis of several molecular properties. Similarly to the transition metal oxides, the bonding between the actinide and oxygen atoms is intermediate between ionic and covalent character. This is well reflected by the natural charges of the actinides and by the Wiberg bond indices (Table 4), indicating a comparable magnitude of ionic and covalent contributions. The actinide charges in the monoxides vary between +1.0 and +1.4 e while those in the dioxides between +1.3 and +2.1 e (the latter range in agreement with the superimposed electron withdrawing effect of two oxygens). The Wiberg bond indices[31] estimating the covalent bond order have values between 1.1 and 1.7 for the monoxides and between 0.9 and 1.9 for the dioxides. The complementary character of the charges and bond indices (taking also into account the limitations of the natural charge and Wiberg models, cf., e.g., ThO and EsO) can be well recognized in the data. The most notable characteristics are (i) the oxides of late actinides are generally substantially more ionic than those of the early actinides; (ii) for most actinides the covalent characters (the Wiberg indices) of the monoxides and dioxides are very close.

The role of the valence orbitals of the An atoms in the bonding can be deduced from the orbital populations given in the last three columns of Table 4. The general trend is the decreasing 6d contribution along the actinide row parallel with an increasing contribution of the 5f orbitals. Similar trends have been reported for other (early) actinide compounds.[37] Sudden changes occur in the trends when the 7s orbitals lose an electron ($7s^2 \rightarrow 7s^1$ from PaO to UO and $7s^1 \rightarrow 7s^0$ from PuO_2 to AmO_2), the electron distributed then between the An (5f and 6d) and oxygen orbitals. The latter increased charge on the oxygen results in an increased ionic character of the bonding (cf., e.g., ThO_2 vs PaO_2 and PuO_2 vs AmO_2). At a detailed inspection of the molecular orbitals, the 7s orbitals with near integer (2 or 1) populations could be recognized as nonbonding lone pairs or lone electrons, respectively. The partial 7s populations of 0.4 e in MdO and NoO mean strong mixing with other (mainly with nonbonding 5f) orbitals.

The 6d population data give straightforward information on their (decreasing) role in the bonding, as they appear exclusively in bonding or antibonding molecular orbitals. In contrast, the populated 5f orbitals form lone pairs (in the late actinides) and lone electrons and in addition are heavily involved in the bonding and antibonding orbitals. For example, from the 8.26-e 5f population of BkO one 5f lone pair and only three lone (nonbonding) 5f electrons could be recognized

dx.doi.org/10.1021/ic300275y | Inorg. Chem. 2012, 51, 4841−4849

Table 4. Selected Molecular Properties[a] of the Ground-State AnO and AnO_2 Species

						population[b]		
An	bond distance	bond angle	vibrational frequencies	charge of An	bond index	5f	6d	7s
ThO	1.833		910	+1.15	1.61	0.36	0.71	1.85
PaO	1.812		932	+1.06	1.73	1.46	0.67	1.87
UO	1.843		844	+1.12	1.54	3.10	0.90	0.94
NpO	1.836		836	+1.10	1.54	4.20	0.81	0.94
PuO	1.830		821	+1.09	1.54	5.31	0.71	0.93
AmO	1.836		781	+1.12	1.43	6.44	0.64	0.84
CmO	1.842		825	+1.14	1.37	7.18	0.79	0.93
BkO	1.835		833	+1.12	1.35	8.26	0.72	0.94
CfO	1.822		833	+1.12	1.32	9.29	0.68	0.94
EsO	1.822		825	+1.14	1.28	10.29	0.66	0.94
FmO	1.850		735	+1.24	1.18	11.56	0.52	0.71
MdO	1.898		673	+1.32	1.12	12.93	0.40	0.37
NoO	1.923		650	+1.36	1.11	13.90	0.36	0.39
LrO	1.871		756	+1.27	1.20	14.00	0.65	1.10
ThO_2[c]	1.898	119.0	820, 766, 155	+2.13	1.58	0.72	1.28	0.03
PaO_2[c]	1.806	180.0	871, 828, 59	+1.70	1.78	1.66	0.99	0.88
UO_2[c]	1.789	180.0	926, 874, 141	+1.53	1.85	2.82	0.97	0.88
NpO_2[c]	1.767	180.0	933, 874, 194	+1.40	1.89	3.99	0.95	0.88
PuO_2[c]	1.748	180.0	933, 863, 183	+1.28	1.91	5.14	0.93	0.88
AmO_2[c]	1.826	180.0	795, 740, 90	+1.84	1.52	6.54	0.74	0.03
CmO_2[c]	1.839	180.0	779, 720, 96	+1.97	1.28	7.41	0.76	0.03
BkO_2	1.820	180.0	791, 725, 152	+1.90	1.26	8.54	0.72	0.03
CfO_2	1.817	180.0	795, 716, 183	+1.89	1.23	9.56	0.69	0.03
EsO_2	1.795	180.0	816, 738, 213	+1.84	1.22	10.68	0.67	0.03
FmO_2	1.791	180.0	816, 730, 221	+1.87	1.20	11.71	0.65	0.02
MdO_2	1.812	180.0	789, 703, 182	+1.88	1.19	12.71	0.59	0.02
NoO_2	1.843	180.0	753, 668, 170	+1.99	0.94	13.62	0.55	0.02
LrO_2	1.940	101.5	686, 271, 114	+1.91	0.98	13.97	0.90	0.24

[a]Distances are given in angstroms, angles in degrees, vibrational frequencies in cm^{-1}, natural charges of the actinides in elementary charge. The vibrational frequencies, in the order they are listed, represent the fundamentals asymmetric stretch, symmetric stretch, and bend, respectively. [b]Population of An valence orbitals in elementary charge. [c]The bond distances, bond angles, and vibrational frequencies were taken from ref 15.

among the molecular orbitals; the rest (3.26 e) appear in the bonding and antibonding orbitals (vide infra in Figure 1).

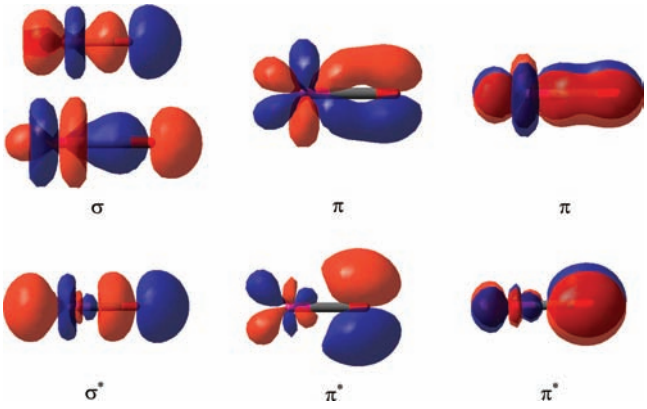

Figure 1. Characteristic Kohn–Sham orbitals of AnO molecules (An atom is on the left-hand side in each plot).

In the following we introduce and analyze the most important Kohn–Sham orbitals in the AnO and AnO_2 species (shown in Figures 1 and 2, respectively) which reveal the main features of the orbital interactions.

In the AnO oxides we found one σ and two π low-energy fully occupied bonding orbitals between An and O (Figure 1). They have in most cases a strong An5f character and a minor

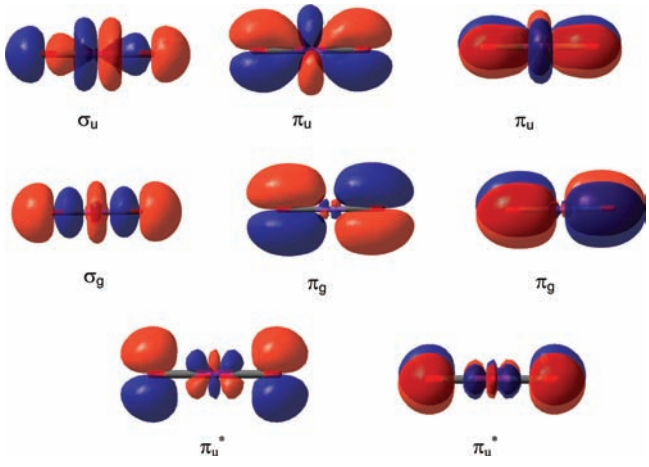

Figure 2. Characteristic Kohn–Sham orbitals of AnO_2 molecules.

O2p contribution. Note that the σ orbitals of ThO to AmO preferentially involve An6dσ rather than An5fσ. The nonbonding orbitals of An5f electrons (pure or with very small O2p contributions) appear at somewhat higher energies than the above-mentioned bonding orbitals. The highest-energy occupied orbitals are antibonding orbitals: the σ^* orbital has dominant An7s and O2p character, while the two π^* orbitals have a strong O2p character and a minor An5f contribution.

dx.doi.org/10.1021/ic300275y | Inorg. Chem. 2012, 51, 4841–4849

The three bonding orbitals are doubly occupied in all the An monoxides. The occupation of the antibonding orbitals begins at NpO with an α electron in a π^* orbital. In AmO both π^* orbitals are occupied by α electrons, while from CmO to LrO all the three antibonding orbitals are occupied by α electrons. β-Occupation of the antibonding orbitals starts at FmO and increases to LrO.

The bonding in the AnO_2 molecules consists of two σ and four π bonding orbitals (Figure 2), doubly occupied in all dioxides from PaO_2. The σ_g orbital is characterized by a major O2p contribution and by minor contributions from An6dσ and An7s. The π_g orbitals have major O2p and minor An6dπ contributions. The σ_u orbital has a major An5fσ and minor O2p character, while the π_u bonding orbitals have major An5fπ and minor O2p contributions. The *gerade* (g) Kohn−Sham orbitals with An6d contribution are lower in energy then the *ungerade* (u) orbitals with An5f contribution in the light actinide dioxides. The energy ordering of these orbitals switches between AmO_2 and CmO_2.

The lower energy of π_u orbitals with respect to π_g in the late actinides indicates the increasing importance of An5f orbitals in the covalent bonding interactions. The general stabilization of the 5f manifold from Th to Lr means gradually decreasing 5f orbital energies in this order. Consequently, the molecular orbitals formed by An5f also have lower orbital energies (unless the contribution of An5f orbitals would decrease in them, but this is not the case here).

The molecular orbitals of ThO_2 and LrO_2 differ considerably from those of the other actinides owing to their different (bent) geometry. In both molecules the contribution of An5f orbitals in the bonding is negligible.

The lowest-energy antibonding orbitals in the dioxides have π_u^* character (Figure 2) consisting mainly of O2p with minor An5fπ contributions. Going from PaO_2 toward NoO_2 the first occupation of a π_u^* orbital by an α electron occurs in AmO_2. Both π_u^* orbitals are occupied by the α electrons from BkO_2, while the β electrons start to occupy them from FmO_2. The antibonding σ^* and π_g^* orbitals are not populated in the ground-state AnO_2 structures.

The population of the various molecular orbitals plays a very important role in the trend of the AnO and AnO_2 bond distances. The geometry information is given in detail in Table 4 and is depicted in Figure 3. In the following we will interpret the most characteristic features of the two curves on the basis of the molecular orbitals. This comparative analysis does not include ThO_2 and LrO_2 because of their bent geometry. Their considerably longer bond distances compared with the other An dioxides can partly be attributed to the repulsion of the oxygens (and of the bonding electron density) getting closer in these geometries than in the linear AnO_2 arrangements.

Before we start with the analysis of the bond distances, we assess first the reliability of our computed geometrical parameters on the basis of some experimental information. In the literature there are accurate equilibrium bond distance data for ThO and UO (r_{ThO} = 1.840 186 13(24) Å;[38] r_{UO} = 1.8383(6) Å[39] obtained by microwave and high-resolution photoelectron spectroscopy, respectively). Compared with our B3LYP data in Table 4, we can see that our calculations underestimate the ThO bond distance by 0.007 Å, while overestimating the UO bond distance by 0.005 Å. (We note that such error is not unusual for actinide oxides; e.g., the CASPT2 method resulted in an overestimation of 0.02 Å for the ThO bond distance.[15,25]) Therefore, we will omit a discussion of minor features of such magnitude in the graphs.

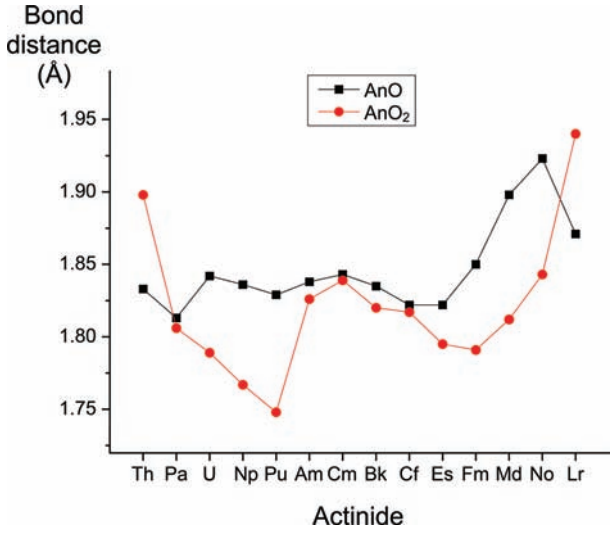

Figure 3. Comparison of bond distances in the actinide mono- and dioxides from B3LYP computations. Data for Th−Cm oxides were taken from ref 22.

The computed bond distances depicted in Figure 3 show a resemblance to a double-well with the saddle point at Cm in both series. It differs obviously from the decreasing trend found for the actinide ionic radii[40] known as "actinide contraction" analogously to the "lanthanide contraction" among 4f elements.[41−43] The "actinide contraction", however, can be manifested only in the strongly ionic bonds. In the oxides the covalent and ionic contributions to the bonding are comparable; thus, the different molecular orbital occupations can readily surpass the electrostatic trend.

On the basis of the molecular orbital occupations we can explain the following significant features in the bond distances: (i) The first is the relatively short bond in PaO. According to the NBO data compiled in Table 4 the bonding in PaO has a larger covalent character, with a larger 5f contribution, than in its neighbors ThO and UO (and subsequently in NpO, PuO, etc.). The smaller radius of the 5f versus 6d orbitals can be one factor responsible for the relatively short PaO bond. We note also the filled $7s^2$ subshell in ThO and PaO, while from UO along the actinide row the 7s is only singly occupied. The closed s subshells have smaller shell radii than the open ones;[44] hence, the $7s^2$ subshell can also enforce some bond-shortening in ThO and PaO with respect to the subsequent AnO species. (ii) The second is the steep increase from EsO to NoO. We showed above that the antibonding orbitals start to be occupied gradually from NpO toward CmO, and in CmO−CfO both the σ^* and the two π^* orbitals are occupied by α electrons. This gradual α-occupation has no considerable effect on the bond distance. The β-occupation of these antibonding orbitals starts from FmO. In fact, in FmO the two π^* orbitals, while in MdO and NoO both the σ^* and the two π^* orbitals are doubly occupied. This double occupation of the antibonding orbitals seems to be the main factor in the increase of the bond distances. The shorter MdO bond distance with respect to that of NoO can be attributed to minor differences in the valence Kohn−Sham orbitals (given in the Supporting Information): these are pure An5f orbitals in NoO, while some of them contain minor contributions from O2p in MdO and FmO. In

dx.doi.org/10.1021/ic300275y | Inorg. Chem. 2012, 51, 4841−4849

these latter orbitals a small overlap between An5f and O2p is observed, resulting in some weak bonding interactions in addition to the ordinary σ and π bonding orbitals. (iii) Third is the shorter bond in LrO. In this molecule doubly occupied σ, π, σ^*, and π^* orbitals as well as pure nonbonding Lr5f orbitals were found. The main difference with respect to the lighter monoxides is that the Lr5f orbital energies (including also σ and π with predominant Lr5f contribution) are about 0.2 hartree lower than those in the other monoxides. This energetic stabilization may result in the shorter LrO bond distance. (iv) Fourth is the gradual decrease from PaO_2 to PuO_2: the six bonding (two σ and four π, cf. Figure 2) orbitals are doubly occupied, while the remaining valence electrons occupy the nonbonding 7s as well as the 5f orbitals. The only difference between the four dioxides appears in the 5f occupation which increases gradually from PaO_2 (0) to PuO_2 (3). As the 5f electrons (similarly to 4f in the lanthanides) poorly shield the nuclear charge from the 6s, 6p, 6d, and 7s electrons, the latter are attracted more efficiently by the nuclear charge increasing from Pa to Pu. This is the actinide analogy of the well-known "lanthanide contraction".[41,43] Accordingly, the magnitude of bond shortening from PaO_2 to PuO_2 agrees well with the decrease in the radii of these An(IV) ions.[40] At the same time the energies of the six bonding orbitals decrease gradually from PaO_2 to PuO_2. The trend breaks at AmO_2, where a considerable change occurs in the electronic structure (vide infra). (v) The fifth is the larger bond distance from AmO_2. From AmO_2 to NoO_2 the single-occupation of the 7s orbital is replaced by occupation of an antibonding orbital. The stabilizing effect of 7s is removed (the energies of the bonding orbitals in AmO_2 are considerably higher than those of PaO_2-to-PuO_2); hence, the bond distance is elongated. (vi) Sixth is the increase from FmO_2 to NoO_2. As mentioned above, from BkO_2 to EsO_2 the two π_u^* orbitals are singly occupied. One of these antibonding orbitals is β-occupied in FmO_2 and MdO_2, while both are completely filled in NoO_2. This explains the longest bond distance for linear AnO_2 in NoO_2. The shorter bond distance in FmO_2 with respect to MdO_2 may be attributed to the mixed character of some Fm5f orbitals with O2p resulting in additional weak bonding contributions (see Supporting Information).

In addition, we note that except for the nonlinear ThO_2 and LrO_2 the dioxides have shorter bond distances than the respective monoxides indicating larger bond strength in the dioxides.

Table 4 also lists the computed harmonic vibrational frequencies for all the actinide oxides dealt with in the present study. The computed anharmonic effects for ThO_2–CmO_2 did not exceed 10 cm^{-1};[15] hence, this magnitude of anharmonicity can be expected for all the oxides in the present study too. The general trend in the stretching frequencies is opposite to that of the bond distances: longer bond distances (hence weaker bonds) are accompanied mostly by smaller vibrational frequencies. A more definite relation cannot be drawn between the two molecular parameters because (beyond the different atomic masses) the vibrational frequency is determined by the potential energy curve around the equilibrium bond distance. The bond distance, however, is related to the bonding at the bond distance only. The most striking case among the present studied molecules is the very low symmetric stretching frequency of LrO_2 indicating an extremely flat potential curve for this fundamental.

Our computed bond dissociation enthalpies (together with available experimental data[6,45]) for the reactions AnO → An + O and AnO_2 → AnO + O are depicted in Figures 4 and 5,

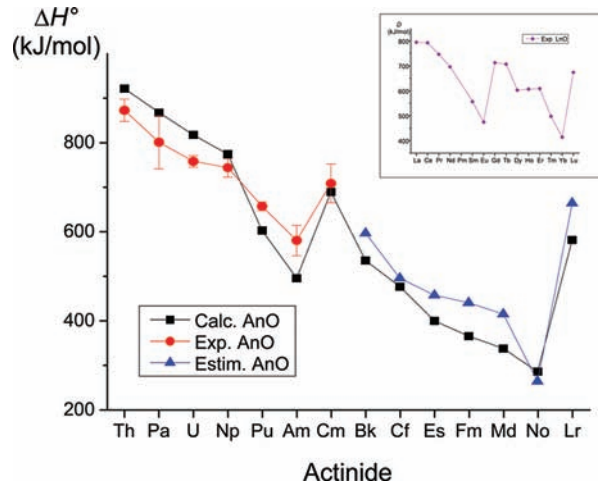

Figure 4. Bond dissociation enthalpies ($\Delta H°$) of AnO from the present B3LYP calculations (–■–), experiment[6] (–●–), and estimations of Haire[13] (–▲–). The trend of the dissociation energies of lanthanide monoxides is in the upper right corner.[46]

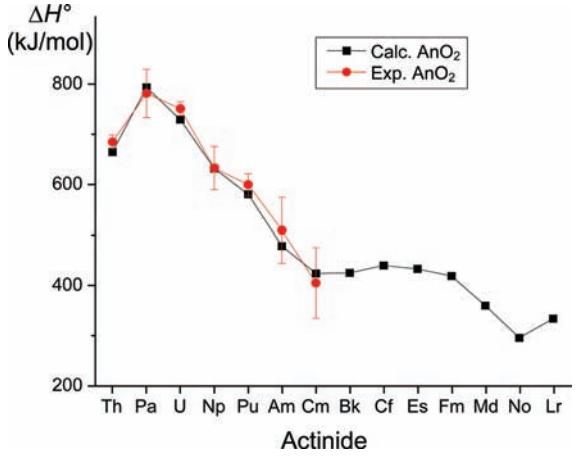

Figure 5. Bond dissociation enthalpies ($\Delta H°$) of AnO_2 (→ AnO + O) from B3LYP calculations (–■–) and experiment[6] (–●–).

respectively, and are compiled in Table 5. Comparison with available experimental data on the early actinide oxides (ThO–CmO and ThO_2–CmO_2) revealed a good agreement with the AnO_2 dissociation enthalpies (average error of ca. 20 kJ/mol), while somewhat less with those of AnO (average error of ca. 50 kJ/mol). In the latter case the computed values fall out of the experimental uncertainty ranges except for CmO. We considered the effect of spin–orbit coupling on the basis of literature data. Computed spin–orbit contributions to dissociation energies are available for AnO_2 (An = Th–Cm).[22] The spin–orbit effects were computed to be negligible for the dissociation of ThO_2, UO_2, and PuO_2, while for PaO_2, NpO_2, AmO_2, and CmO_2 the values −33, −4, −21, and +4 kJ/mol, respectively, have been reported. Using the spin–orbit data of the latter molecules, our corrected DFT dissociation enthalpies would still remain within the experimental uncertainty range.

Nevertheless, the experimental trends for both the AnO and AnO_2 molecules are very well reproduced by our computations.

dx.doi.org/10.1021/ic300275y | Inorg. Chem. 2012, 51, 4841–4849

Table 5. Dissociation Energetics[a] of AnO and AnO_2 Species

An	$\Delta H°_{0calc}$	$\Delta H°_{298calc}$	$\Delta G°_{298calc}$	$\Delta H°_{298exp}$[b]	$\Delta H°_{0estim}$[c]
ThO	914	920	890	872 ± 25[d]	
PaO	861	867	839	801 ± 59	
UO	811	817	791	758 ± 13[d]	
NpO	768	774	748	744 ± 21	
PuO	598	604	577	658 ± 10[d]	
AmO	492	498	471	582 ± 34	550
CmO	684	690	663	709 ± 43	
BkO	537	543	517		598
CfO	479	485	459		498
EsO	403	409	383		460
FmO	369	373	347		443
MdO	341	349	323		418
NoO	290	295	269		268
LrO	583	588	562		665
ThO_2	658	664	632	684 ± 14[d]	
PaO_2	787	792	756	780 ± 48	
UO_2	723	728	689	750 ± 14[d]	
NpO_2	626	631	590	632 ± 43	
PuO_2	575	580	533	599 ± 22[d]	
AmO_2	475	478	441	509 ± 65	
CmO_2	421	424	388	405 ± 70	
BkO_2	420	425	386		
CfO_2	434	440	391		
EsO_2	427	433	392		
FmO_2	413	419	379		
MdO_2	354	360	303		
NoO_2	291	296	257		
LrO_2	330	334	305		

[a]Bond dissociation ($AnO_2 \rightarrow AnO + O$, $AnO \rightarrow An + O$) enthalpies at 0 K ($\Delta H°_{0calc}$) and 298 K ($\Delta H°_{298calc}$) and Gibbs free energies at 298.15 K ($\Delta G°_{298calc}$) in kJ/mol. The $\Delta G°_{298calc}$ data do not include the contribution of excited electronic states. [b]From ref 6. A few data have older literature origin, see footnote [d]. [c]From ref 13. [d]From ref 45.

This suggests that the computed trends for the Bk–Lr oxides can also be reliable. For the latter oxides we can expect a similar average error of the computations as found for the early actinides.

We note the resemblance of the trends in the AnO and LnO dissociation energies (the latter[46] is depicted in the upper right corner of Figure 4). Both curves decrease gradually until the middle of the f-element row, where a sudden raise occurs followed by a gradual decrease again. The trend in the experimental gas-phase dissociation energies of the Ln monoxides has been interpreted in terms of the promotion energies for the $4f^n \rightarrow 5d^14f^{n-1}$ lanthanide electronic transitions preparing in this way a divalent configuration in the metal center.[46−48] A successful model has been developed for the prediction of the dissociation energies, in which the dissociation energies of LaO, CeO, GdO, and LuO (lanthanides with $6s^25d^14f^n$ electronic ground states) formed a common baseline across the series, and the dissociation energies of the other lanthanide monoxides (lanthanides with $6s^24f^n$ electronic ground states) fell below this baseline by the amount of the above-mentioned promotion energies. Using the electronic transition energies of the free gaseous lanthanide atoms, the predicted dissociation energies were within experimental error for most LnO molecules.[13,14,46,48]

This model has been extended for actinide monoxides by Haire.[13] The baseline in the actinide monoxides corresponds to the $7s^16d^25f^n$ configuration except for Th and Pa for which the $7s^26d^25f^{n-1}$ configuration is relevant. The model worked quite well for lanthanide monoxides and for the oxides of early actinides, for which experimental data are available.[13,14] Using the present computed dissociation enthalpies we are able to assess the performance of Haire's model for the late actinide monoxides. As it can be seen in Figure 4, the agreement is very good, the average deviation being comparable to the differences between experiment and computations of the early actinide monoxides. Hence the present DFT results provide a nice validation of the simple model used by Haire.[13]

The general character of the dissociation enthalpies corresponds to a decreasing trend along the actinide row. Deviations from a gradual decrease can be observed at the ends (Th and Lr) and in the middle of the row. As the dissociation enthalpies are determined by the stability of both the dissociating molecules and dissociation products, we have to consider both factors in the interpretations.

First of all we have to distinguish between intrinsic bond strength and bond dissociation energy. The former can be related to the bond distance, as weaker bonds are generally associated with larger interatomic distances and vice versa. The bond strength is related also to the so-called vertical dissociation energy, where the dissociation products maintain the electronic structure they had in the original molecule. However, this electronic structure corresponds very often to an excited state for the dissociation products; hence, they relax immediately to their electronic ground state. The sum of these processes gives the adiabatic dissociation energy, which is generally obtained by experiments. In the present paper we computed and deal with this latter (adiabatic) dissociation energy.

We can expect a correlation of the dissociation enthalpies with the bond distances when the electronic structure of the actinide atom in the dissociation product is similar to that in the original oxide. Inspecting the data of the monoxides, the considerably larger dissociation energy of LrO as compared to the neighbors NoO, MdO, etc., can partly be attributed to the larger strength of the LrO bond indicated by its shorter bond distance (cf. Figure 3). In addition, the less stable electron configuration of the Lr atom ($5f^{14}7s^27p^1$) compared with the closed-shell configuration of No ($5f^{14}7s^2$) contributes also to the large dissociation energy of LrO. The effect of the electronic structure of the dissociation products is manifested more clearly in the case of NpO, AmO, and BkO. These monoxides have nearly identical bond distances (cf. Table 4); therefore, the strong variation in their dissociation enthalpies is mainly determined by the electron configurations of the actinide atoms. Indeed, the small dissociation energy of AmO is in good agreement with the very stable $5f^77s^2$ configuration of ground-state Am compared to the other actinide atoms (Np $5f^46d^17s^2$; Bk $5f^97s^2$).

We can find some correlations also between the dissociation enthalpies of the dioxides and the bond distances. In Figure 5 we can observe similar dissociation enthalpies for AmO_2 to FmO_2, which refers to similar bond strengths of the mono- and dioxides of these actinides. This feature is also manifested in the close bond distances of the mono- and dioxides from An = Am to Es (cf. Figure 3). On the other hand, the large dissociation enthalpies of UO_2, NpO_2, and PuO_2 can partly be related to their considerably shorter bond distances (indicating considerably stronger bonds) as compared to the monoxide counterparts. The data of the other dioxides (particularly

dx.doi.org/10.1021/ic300275y | Inorg. Chem. 2012, 51, 4841−4849

PaO_2, MdO_2, and NoO_2) deviate considerably from the correlation model, supporting that the bond distance is not a general measure of the bond strength.

4. CONCLUSIONS

In the present paper we have reported for the first time the computed electronic ground states and some important molecular properties (geometry, vibrational frequencies, natural charges, dissociation enthalpies) for the mono- and dioxides of late actinides An = Bk−Lr. In addition, we have evaluated trends in the bond distances and dissociation enthalpies for the mono- and dioxides of the actinide row. The most important characteristics can be summarized as follows: (i) On the basis of the computed natural charges and Wiberg bond indices the ionic and covalent contributions of bonding are of comparable strength. (ii) We have identified three (one σ and two π) and six (two σ and four π) bonding orbitals in the AnO and AnO_2 molecules, respectively, which are fully occupied in the ground states of the studied oxides. The antibonding orbitals (π^*) are first occupied from NpO and AmO_2 by the α electrons, with occupation gradually increasing along the actinide row. The α-filled antibonding orbitals start to be occupied by β electrons from EsO and FmO_2. The above features reflect a complex bonding situation in actinide oxides. As the populated antibonding orbitals cancel the effect of bonding orbitals, the formal bond order is lower than three in the late actinide oxides. The primary bonding orbitals are accompanied in some cases by minor bonding interactions in other (formally nonbonding) orbitals. (iii) The bond distances of most of the dioxides are somewhat shorter than those of the monoxides. The trend in the whole actinide row resembles a double-well with Cm at the saddle-point. The main features of the curves can be explained by the different occupations of the Kohn−Sham orbitals. While the single occupation of antibonding orbitals had no substantial effect on the bond distances, the double occupation lengthened them considerably. (iv) The dissociation enthalpies of both oxide series show an overall decreasing trend along the actinide row. The most characteristic features can be interpreted on the stability conditions of the dissociating molecules and products. The stability of the molecule is characterized by the bond strength, with another term, by the interaction energy (sum of ionic and covalent contributions) between the two fragments of the molecule. The bond strength is reflected by the bond distance, though a direct correlation cannot be drawn because the ionic and covalent interactions have generally somewhat different optimal interatomic distances. In addition to the bond strength, the dissociation energy depends strongly on the electronic structure of the dissociation products, which are often different from that in the molecule.

The present study demonstrated the very good performance of the B3LYP exchange-correlation functional in conjunction with the applied relativistic effective core potential and extended triple-ζ valence basis set. We note also the remarkable predictive reliability of the model used by Haire[13] nearly 20 years ago.

■ ASSOCIATED CONTENT

Supporting Information

Computed molecular geometries and characteristics of the electronic structure of all the electronic states determined in this study. The Kohn−Sham orbitals representing minor An5f−O2p overlaps in a few oxides. This material is available free of charge via the Internet at http://pubs.acs.org.

■ AUTHOR INFORMATION

Corresponding Author

*E-mail: attila.kovacs@ec.europa.eu.

Notes

The authors declare no competing financial interest.

■ ACKNOWLEDGMENTS

The Hungarian Scientific Research Foundation (OTKA 75972) is acknowledged for financial support. The authors thank Dr. J. Rabone for advice.

■ REFERENCES

(1) Krebs, R. *The History and Use of our Earth's Chemical Elements*; Greenwood Publishing Group: Westport, CT, 2006.
(2) *The Chemistry of the Actinide and Transactinide Elements*; Morss, L. R., Edelstein, N. M., Fuger, J., Eds.; Springer: Dordrecht, The Netherlands, 2006.
(3) Heaven, M. C. *Phys. Chem. Chem. Phys.* **2006**, *8*, 4497−4509.
(4) Heaven, M. C.; Gibson, J. K.; Marçalo, J. Molecular Spectroscopy and Reactions of Actinides in the Gas Phase and Cryogenic Matrices. In *The Chemistry of the Actinide and Transactinide Elements*; Edelstein, N. M., Fuger, J., Morss, L. R., Eds.; Springer: Dordrecht, The Netherlands, 2011; Vol. *6*, pp 4079−4156.
(5) Morss, L. R. *J. Less Common. Metals* **1983**, *93*, 301−321.
(6) Marcalo, J.; Gibson, J. K. *J. Phys. Chem. A* **2009**, *113*, 12599−12606.
(7) Blaise, J.; Wyart, J.-F. *Energy Levels and Atomic Spectra of Actinides, International Tables of Selected Constants*; CNRS: Paris, 1992; Vol. *20*.
(8) Blaise, J.; Wyart, J.-F. *Selected Constants, Energy Levels and Atomic Spectra of Actinides*; Laboratoire Aimé Cotton, CNRS: Paris; http://www.lac.u-psud.fr/Database/Contents.html.
(9) Erdmann, N.; Nunnemann, M.; Eberhardt, K.; Herrmann, G.; Huber, G.; Köhler, S.; Kratz, J. V.; Passler, G.; Peterson, J. R.; Trautmann, N.; Waldek, A. *J. Alloys Compd.* **1998**, *271−273*, 837−840.
(10) Greenwood, N. N.; Earnshaw, A. *Chemistry of the Elements*; Butterworth-Heinemann: Oxford, 1997.
(11) Cotton, F. A.; Wilkinson, G.; Murillo, C. A.; Bochmann, M. *Advanced Inorganic Chemistry*, 6th ed.; Wiley: New York, 1999.
(12) Nugent, L. J.; Burnett, J. L.; Morss, L. R. *J. Chem. Thermodyn.* **1973**, *5*, 665−678.
(13) Haire, R. G. *J. Alloys Compd.* **1994**, *213/214*, 185−191.
(14) Gibson, J. K. *J. Phys. Chem. A* **2003**, *107*, 7891−7899.
(15) Kovács, A.; Konings, R. J. M. *J. Phys. Chem. A* **2011**, *115*, 6646−6656.
(16) Dolg, M. Lanthanides and Actinides. In *Encyclopedia of Computational Chemistry*; Schleyer, P. v. R., Allinger, N. L., Clark, T., Gasteiger, J., Kollman, P. A., Schaefer, H. F., III, Schreiner, P. R., Eds.; Wiley: Chichester, U.K., 1998; pp 1478−1486.
(17) Dolg, M.; Cao, X. Computational Methods: Lanthanides and Actinides. In *Computational Inorganic and Bioinorganic Chemistry*; Solomon, E. I., Scott, R. A., King, R. B., Eds.; Wiley: Chichester, U.K., 2009.
(18) Lenthe, E. v.; Baerends, E. J. *J. Comput. Chem.* **2003**, *24*, 1142.
(19) Küchle, W.; Dolg, M.; Stoll, H.; Preuss, H. *J. Chem. Phys.* **1994**, *100*, 7535−7542.
(20) Cao, X. Y.; Dolg, M.; Stoll, H. *J. Chem. Phys.* **2003**, *118*, 487−496.
(21) Cao, X. Y.; Dolg, M. *THEOCHEM* **2004**, *673*, 203−209.
(22) Averkiev, B.; Mantina, M.; Valero, R.; Infante, I.; Kovács, A.; Truhlar, D. G.; Gagliardi, L. *Theor. Chem. Acc.* **2011**, *129*, 657−666.
(23) Becke, A. D. *J. Chem. Phys.* **1993**, *98*, 5648.
(24) Lee, C.; Yang, W.; Parr, R. G. *Phys. Rev. B* **1988**, *37*, 785.
(25) Infante, I.; Kovács, A.; La Macchia, G.; Shahi, A. R. M.; Gibson, J. K.; Gagliardi, L. *J. Phys. Chem. A* **2010**, *114*, 6007−6015.

(26) La Macchia, G.; Infante, I.; Raab, J.; Gibson, J. K.; Gagliardi, L. *Phys. Chem. Chem. Phys.* **2008**, *10*, 7278−7283.
(27) Frisch, M. J.; Trucks, G. W.; Schlegel, H. B.; Scuseria, G. E.; Robb, M. A.; Cheeseman, J. R.; Montgomery, J. A., Jr.; Vreven, T.; Kudin, K. N.; Burant, J. C.; Millam, J. M.; Iyengar, S. S.; Tomasi, J.; Barone, V.; Mennucci, B.; Cossi, M.; Scalmani, G.; Rega, N.; Petersson, G. A.; Nakatsuji, H.; Hada, M.; Ehara, M.; Toyota, K.; Fukuda, R.; Hasegawa, J.; Ishida, M.; Nakajima, T.; Honda, Y.; Kitao, O.; Nakai, H.; Klene, M.; Li, X.; Knox, J. E.; Hratchian, H. P.; Cross, J. B.; Bakken, V.; Adamo, C.; Jaramillo, J.; Gomperts, R.; Stratmann, R. E.; Yazyev, O.; Austin, A. J.; Cammi, R.; Pomelli, C.; Ochterski, J. W.; Ayala, P. Y.; Morokuma, K.; Voth, G. A.; Salvador, P.; Dannenberg, J. J.; Zakrzewski, V. G.; Dapprich, S.; Daniels, A. D.; Strain, M. C.; Farkas, O.; Malick, D. K.; Rabuck, A. D.; Raghavachari, K.; Foresman, J. B.; Ortiz, J. V.; Cui, Q.; Baboul, A. G.; Clifford, S.; Cioslowski, J.; Stefanov, B. B.; Liu, G.; Liashenko, A.; Piskorz, P.; Komaromi, I.; Martin, R. L.; Fox, D. J.; Keith, T.; Al-Laham, M. A.; Peng, C. Y.; Nanayakkara, A.; Challacombe, M.; Gill, P. M. W.; Johnson, B.; Chen, W.; Wong, M. W.; Gonzalez, C.; Pople, J. A. *Gaussian 03*, revision D.01; Gaussian, Inc.: Wallingford, CT, 2004.
(28) Frisch, M. J.; Trucks, G. W.; Schlegel, H. B.; Scuseria, G. E.; Robb, M. A.; Cheeseman, J. R.; Scalmani, G.; Barone, V.; Mennucci, B.; Petersson, G. A.; Nakatsuji, H.; Caricato, M.; Li, X.; Hratchian, H. P.; Izmaylov, A. F.; Bloino, J.; Zheng, G.; Sonnenberg, J. L.; Hada, M.; Ehara, M.; Toyota, K.; Fukuda, R.; Hasegawa, J.; Ishida, M.; Nakajima, T.; Honda, Y.; Kitao, O.; Nakai, H.; Vreven, T.; Montgomery, J. A., Jr.; Peralta, J. E.; Ogliaro, F.; Bearpark, M.; Heyd, J. J.; Brothers, E.; Kudin, K. N.; Staroverov, V. N.; Keith, T.; Kobayashi, R.; Normand, J.; Raghavachari, K.; Rendell, A.; Burant, J. C.; Iyengar, S. S.; Tomasi, J.; Cossi, M.; Rega, N.; Millam, J. M.; Klene, M.; Knox, J. E.; Cross, J. B.; Bakken, V.; Adamo, C.; Jaramillo, J.; Gomperts, R.; Stratmann, R. E.; Yazyev, O.; Austin, A. J.; Cammi, R.; Pomelli, C.; Ochterski, J. W.; Martin, R. L.; Morokuma, K.; Zakrzewski, V. G.; Voth, G. A.; Salvador, P.; Dannenberg, J. J.; Dapprich, S.; Daniels, A. D.; Farkas, O.; Foresman, J. B.; Ortiz, J. V.; Cioslowski, J.; Fox, D. J. *Gaussian 09*, Revision B.01; Gaussian, Inc.: Wallingford, CT, 2010.
(29) Universität Stuttgart, Institut für Theoretische Chemie, http://www.theochem.uni-stuttgart.de/.
(30) Dunning, T. H., Jr. *J. Chem. Phys.* **1989**, *90*, 1007−1023.
(31) Wiberg, K. B. *Tetrahedron* **1968**, *24*, 1083.
(32) Reed, A. E.; Curtiss, L. A.; Weinhold, F. *Chem. Rev.* **1988**, *88*, 899.
(33) Sannigrahi, A. B.; Kar, T. *J. Chem. Educ.* **1988**, *65*, 674−676.
(34) Mayer, I. *J. Comput. Chem.* **2007**, *28*, 204−221.
(35) Boys, S. F.; Bernardi, F. *Mol. Phys.* **1970**, *19*, 553.
(36) Simon, S.; Duran, M.; Dannenberg, J. J. *J. Chem. Phys.* **1996**, *105*, 11024.
(37) Kirker, I.; Kaltsoyannis, N. *Dalton Trans.* **2011**, *40*, 124−131.
(38) Dewberry, C. T.; Etchison, K. C.; Cooke, S. A. *Phys. Chem. Chem. Phys.* **2007**, *9*, 4895−4897.
(39) Kaledin, L. A.; McCord, J. E.; Heaven, M. C. *J. Mol. Spectrosc.* **1994**, *164*, 27−65.
(40) Edelstein, N. M.; Fuger, J.; Katz, J. J.; Morss, L. R. Summary and Comparison of Properties of the Actinide and Transactinide Elements. In *The Chemistry of the Actinide and Transactinide Elements*; Edelstein, N. M., Fuger, J., Morss, L. R., Eds.; Springer: Dordrecht, The Netherlands, 2006; Vol. *3*, pp 1753−1835.
(41) Cotton, F. A.; Wilkinson, G. *Advanced Inorganic Chemistry*; Wiley: New York, 1988.
(42) Wang, S. G.; Schwarz, W. H. E. *J. Phys. Chem.* **1995**, *99*, 11687−11695.
(43) Hargittai, M. *Chem. Rev.* **2000**, *100*, 2233−2301.
(44) Winter, M. *WebElements*; The University of Sheffield and WebElements Ltd.: Sheffield, U.K., 1993−2011;http://www.webelements.com.
(45) Konings, R. J. M.; Morss, L. R.; Fuger, J. Thermodynamic Properties of Actinides and Actinide Compounds. In *The Chemistry of the Actinide and Transactinide Elements*; Edelstein, N. M., Fuger, J., Morss, L. R., Eds.; Springer: Dordrecht, The Netherlands, 2006; Vol. *4*, pp 2113−2224.
(46) Dulick, M.; Murad, E.; Barrow, R. F. *J. Chem. Phys.* **1986**, *85*, 385−390.
(47) Ames, L. L.; Walsh, P. N.; White, D. *J. Phys. Chem.* **1967**, *71*, 2707−2718.
(48) Murad, E.; Hildenbrand, D. L. *J. Chem. Phys.* **1980**, *73*, 4005−4011.
(49) Gdanitz, R. J.; Ahlrichs, R. *Chem. Phys. Lett.* **1988**, *143*, 413−420.